Prediction of Performance Degradation Due to Grain Coarsening Effects in Solid Oxide Fuel Cells

ECS Transactions, 78 (1) 2323-2336 (2017)
10.1149/07801.2323ecst ©The Electrochemical Society

Prediction of Performance Degradation due to Grain Coarsening Effects in Solid Oxide Fuel Cells

Jerry Mason[a,b], Ismail Celik[a,c], Shiwoo Lee[a,d], Harry Abernathy[a,d], Gregory Hackett[a]

[a] National Energy Technology Laboratory, U.S. Department of Energy, Morgantown WV
[b] Oak Ridge Associated Universities, Oak Ridge, Tennessee, USA
[c] West Virginia University, Morgantown, WV, USA
[d] AECOM, Morgantown, WV, USA

Long term degradation of solid oxide fuel cells (SOFCs) is one of the biggest impediments to commercialization. Physics based models which can predict long term degradation can be crucial time and money saving tools. At the cell level, one of the primary modes of degradation comes from grain coarsening and the resulting changes in microstructure properties. In this study, a multi-physics model of a single fuel cell is presented which aims to predict performance loss as a function of time and temperature caused by coarsening in the electrodes of an LSM-YSZ/YSZ/Ni-YSZ SOFC. Microstructural properties are updated as a function of time from their initial values using functional relations derived from data obtained experimentally and from phase field models. Performance change over time predicted by the model is compared to experimental data and a study is performed on the effect temperature has on the degradation rate due to coarsening.

Introduction

Grain coarsening occurs when two or more particles are in contact with one another under high temperature conditions (1) (2) (3). Over time, the two particles will combine into a new shape with the minimum grain boundary and surface energy. In the case of SOFCs, the electrode materials undergo coarsening, especially during long term operations and at relatively high temperatures. The rate of coarsening is determined by the temperature and initial particle sizes (curvature) among other factors. Small particles coarsen more quickly, and coarsening occurs more rapidly at higher temperatures. At the same time, overall cell performance is better at higher temperatures and key properties such as triple phase boundary density and interfacial area densities are maximized when particle sizes are smallest. Because of this conflict, cells operating at high temperature with finer initial grain sizes tend to degrade more quickly and may lose performance advantages over cells operated at lower temperatures with larger initial grain sizes in the long term. Therefore, there must be some balance between operating conditions and initial microstructure which yields the best long term performance. Due to the large amount of time and expense required to experimentally test SOFC degradation (on the order of thousands of hours) it would be beneficial to instead use physics based computational models that consider experimental data in order to predict degradation patterns reasonably quickly.

For this study, hydrogen fuel is considered with the primary focus being on the microstructural changes within the SOFC electrodes caused by grain coarsening. A multi-physics model is presented which can predict changes in cell performance based on the evolution of the microstructure properties. This model is applied to a commercial button cell which has been characterized at numerous temperatures and then another cell from the same batch is operated for an extended period at 750°C, 0.25 A/cm^2 to study degradation rate. Microstructural properties of a similar cell from the same manufacturer have been obtained using plasma focus ion-beam (PFIB) microscopy. By calibrating the model to baseline (after preconditioning) performance data at different temperatures, temperature dependence is derived for certain kinetic properties for the cell. Grain coarsening is modelled using Ostwald ripening with parameters which were derived from experiments by Kennouche et al (4) (5). The model for triple phase boundary (TPB) density evolution based on grain growth is also taken from this reference. Conciliatory property models based on changes in average particle size are derived based on additional experimental data from Simwonis (6) including phase tortuosity, conductivity and interfacial area densities. The coarsening model is then combined with the Multiphysics model to predict how much degradation occurs due to grain coarsening depending on operating temperature and initial microstructural properties (average grain sizes, volume fractions, etc.).

Experiments

The button cells used for the experiment are commercial anode-supported fuel cells from MSRI (Salt Lake City, UT). As schematically presented in Figure 1, a 10 μm-thick YSZ electrolyte with the diameter of 25.4 mm is supported by an approximately 750 μm-thick Ni-YSZ anode, which includes 20 μm-thick active layer at the interface with the electrolyte. The cathode with the diameter of 16 mm is composed of an active layer of LSM-YSZ (20 μm thick) and a LSM support layer (30 μm thick).

For electrochemical performance tests, cells were placed on an alumina flange with mica sealant on both electrodes. Electrical connections were made with Pt mesh and Pt paste for the cathode and Pt mesh and Ni paste for the anode.

The cell tested at various temperatures was heated up to 650°C under N_2 for anode and air for cathode with the flow rate of 400 sccm each. After temperature was stabilized, wet (3% H_2O) H_2 fuel was injected to the anode while increasing relative content to nitrogen stepwise over 4 hrs. After 20hrs exposure to pure hydrogen, constant current density of 0.25 A/cm^2 was applied to the cell using a DC electric load (Agilent N3301A) for 24 hrs before measuring impedance. Impedance spectra were obtained under various DC bias currents (0–0.5 A/cm^2) with a frequency range of 0.05 to 100 kHz and a 10–75 mA amplitude perturbation using a frequency response analyzer (Solartron 1455A) and a potentiostat/galvanostat (Solartron 1470E). Impedance spectra were repeatedly measured while increasing the operation temperature up to 850°C with the step of 50°C and stabilizing the cell at each temperature for 24 hrs. The Nyquist plot of the impedance are shown in Figure 5 and polarization curves are shown in Figure 6.

The cell operated for extended period of time was directly heated up to 750°C and tested for 775 h under an applied current of 0.25 A/cm^2. Impedance spectra were

intermittently obtained with the same parameters described previously. During this time, the cell experiences a degradation rate of 2.35%/1000hrs as shown in Figure 8.

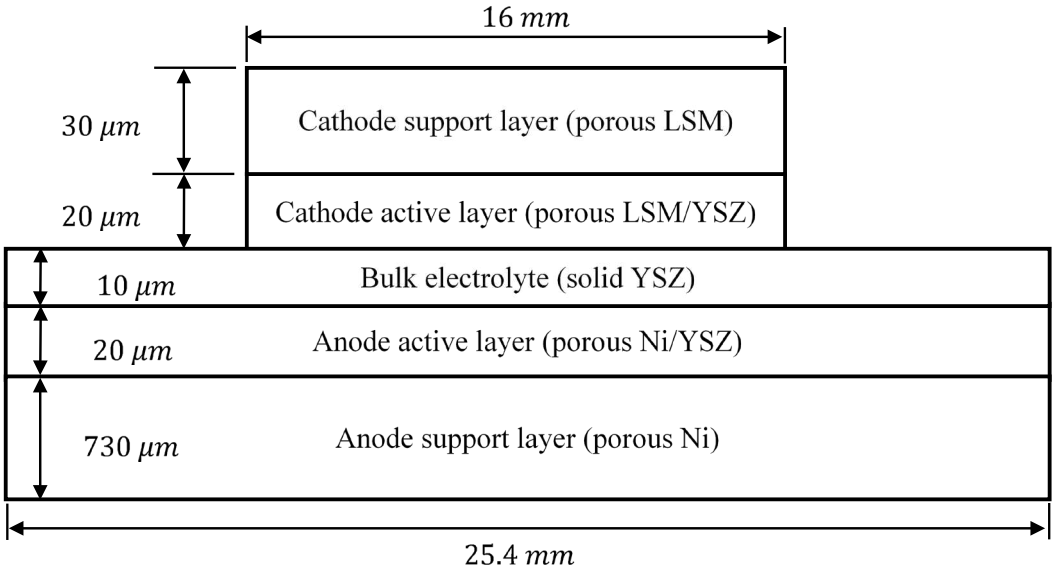

Figure 1. Cell Geometry.

Model

The multi-physics model being applied is an adapted version of the one presented by Yang et al (7) (also see (8)) which was built upon earlier work from the same group (9) (10). In that work, a method was developed which used experiments in conjunction with simulations to derive certain model parameters and analyze cell performance. A similar approach is applied here. This model incorporates realistic micro-structural properties changing through the thickness of the electrodes, specifically between the active and current collecting (support) layers. In the current study, a coarsening model is developed and applied which predicts how these properties will evolve over time and how these changes will affect long term performance.

Governing Equations

The transient forms of the charge conservation equations are applied, which considers the double layer capacitance, current due to charge transport and Faradaic current density (i_F). The electrode materials are treated as mixed ionic-electronic conductors. The charge conservation for the electronic conducting phases is given by (7) (11) (12) (13):

$$a_s^{eff} C_{DL} \frac{\partial(\varphi_e - \varphi_i)}{\partial t} + \nabla \cdot \left(-\sigma_e^{eff} \nabla \varphi_e\right) = i_F \quad [1]$$

The charge transport in the electrolyte phase is solved for using:

$$a_s^{eff} C_{DL} \frac{\partial(\varphi_i - \varphi_e)}{\partial t} + \nabla \cdot \left(-\sigma_i^{eff} \nabla \varphi_i\right) = -i_F \quad [2]$$

Where the effective conductivity is calculated from the tortuosity and volume fraction of the conducting phase (14) (15) from:

$$\sigma_{\phi}^{eff} = \sigma_{\phi}(V_{\phi}/\tau_{\phi}) \quad [3]$$

In the bulk electrolyte, where no electrode material is present, equation [2] simplifies to:

$$\nabla \cdot \left(-\sigma_i^{eff} \nabla \varphi_i\right) = 0 \quad [4]$$

Mass transport in the gas phase is modelled using Fick's diffusion, if gas is transported only via diffusion through the pores:

$$V_p \frac{\partial c_{\phi}}{\partial t} = \nabla \cdot \left(D_{\phi}^{eff} \nabla c_{\phi}\right) - S_{\phi} \quad [5]$$

The diffusion coefficient is calculated considering the Knudsen diffusion, binary molecular diffusion and the pore tortuosity (16) (17) from:

$$D_{\phi}^{eff} = \frac{V_p}{\tau^2}\left(\frac{1 - \beta_{\phi,m} y_{\phi}}{D_{\phi,m}} + \frac{1}{D_{\phi,K}}\right) \quad [6]$$

The governing equations are discretized in three dimensions using the finite volume method in space and solved via an in-house FORTRAN program called DREAM SOFC (18) (19).

Electrochemical Model

To calculate the faradaic current and the source term in the mass transport equation, the Butler-Volmer equation presented by Yang et al (7) is applied for both the anode and cathode.

$$i_{Fa} = i_{0a} l_{TPB,a} \left(P_{H_2}\right)^a \left(P_{H_2O}\right)^b \{exp\left[\frac{\alpha n F \eta_a}{RT}\right] - exp\left[-\frac{(1-\alpha) n F \eta_a}{RT}\right] \quad [7]$$

$$i_{Fc} = i_{0c} l_{TPB,c} \left(P_{O_2}\right)^m \{exp\left[\frac{\alpha n F \eta_c}{RT}\right] - exp\left[-\frac{(1-\alpha) n F \eta_c}{RT}\right] \quad [8]$$

The exponents a, b and m for gas species partial pressure dependence were previously determined by Yang et al (7) by a procedure which used experimental data for performance of a cell with different applied fuel and air concentrations. One difference from Yang et al is that the exchange current density is defined per triple phase boundary length density (l_{TPB}), so that performance changes due to variations in l_{TPB} can be predicted. The anodic and cathodic overpotentials are defined by $\eta_a = (\varphi_a - \varphi_i) - \eta_{eq}$ and $\eta_c = (\varphi_c - \varphi_i) - \eta_{eq}$ respectively.

Coarsening Model

The basis of this model comes from the prediction of average particle size growth as a function of time and temperature within the electrodes. Kennouche et al (5) performed experiments in which several similarly manufactured Ni/YSZ SOFC functional layers are exposed to high temperatures (1000-1200°C) for 500hrs and at 1150°C for various times up to 700 hrs. All the cells were first pre-conditioned at 1100C for 100hrs to eliminate the initial rapid morphological changes from consideration. Reconstruction of transmission X-ray microscopy data is used to investigate morphological differences between the cells and this data is used to derive parameters for an Ostwald ripening model with temperature dependent surface diffusion coefficients for each phase (via an Arrhenius relation):

$$d_{\phi}^{4} - d_{\phi,0}^{4} = K_{D,\phi}\Delta t \quad [9]$$

Where:

$$K_{D,\phi} = K_{D_0,\phi} e^{-\frac{E_{A,\phi}}{\kappa_a T}} \quad [10]$$

Kennouche applies an algorithm based on least median of square regression to obtain the fitting parameters of E_A and K_{D_0} for both Ni and YSZ data. Due to the relatively small sample size a range of values which correspond to a 5% fluctuation in R^2 were presented (maximum values being 0.957 for Ni and 0.94 for YSZ). For the purposes of this study, the parameters which produce the fastest degradation of TPB density are chosen from this range, as this will likely overestimate degradation rather than underestimate it. These parameters are listed in Table 1.

Table 1. Grain coarsening parameters (5)

PARAMETER	VALUE	UNIT
$K_{D_0,YSZ}$	$6.03E-21$	m^4/s
$K_{D_0,Ni}$	$4.11E-23$	m^4/s
$E_{A,YSZ}$	3.09	eV
$E_{A,Ni}$	2.33	eV

Similar parameters are applied to LSM in the cathode as are used for Ni in the anode. This is of course not accurate, but it is probably a conservative over-estimation as LSM seems to coarsen more slowly. This was decided based on a lack of the necessary data needed to derive similar parameters for LSM. Grain coarsening of LSM is believed to be mostly controlled by manganese diffusivity which is similar in magnitude to self-diffusivity of Ni within the typical operating temperature range of SOFCs (20) (21). However, it is suspected that Ni coarsening is more strongly influenced by surface diffusion, which is five orders of magnitude faster than bulk (5) (22) or by gas phase transport (23). Neither of these mechanisms seem to occur within LSM, so it can be assumed that applying the parameters for nickel will yield a conservative overestimation for LSM. Some studies have shown that LSM coarsening is more strongly dependent on the applied current density than operating temperature (24) (25), which is beyond the scope of the current study.

Material Property Models

Kennouche et al (5) shows that using Ostwald ripening with the aforementioned parameters in conjunction with a geometrical sphere-packing model of a composite electrode that the evolution of TPB density can be predicted relatively well using the equation:

$$l_{TPB} = l^0_{TPB} \frac{d^3_{e,0}}{d_{i,0}} \cdot \frac{d_i}{d^3_e} \quad [11]$$

This model equation was derived under the assumption that the average nickel (or LSM) particle sizes are larger than YSZ, which is usually the case.

Conciliatory property models for interfacial area density (a_s^{eff}), average pore size (d_p) and phase tortuosity (τ_i) are derived as functions of average particle size and volume fraction of each phase to best represent experimental data. Using area density data from Kennouche et al, a power law type model is used to approximate how surface area density changes with average particle size:

$$a_\phi = a_{\phi,0} \left(\frac{d_{\phi,0}}{d_\phi} \right)^{n_{area}} \quad [12]$$

It was found that an exponent of $n_{area} = 1$ resulted in a good fit with the normalized Ni surface area density data especially as a function of both time and temperature as shown in Figure 2.

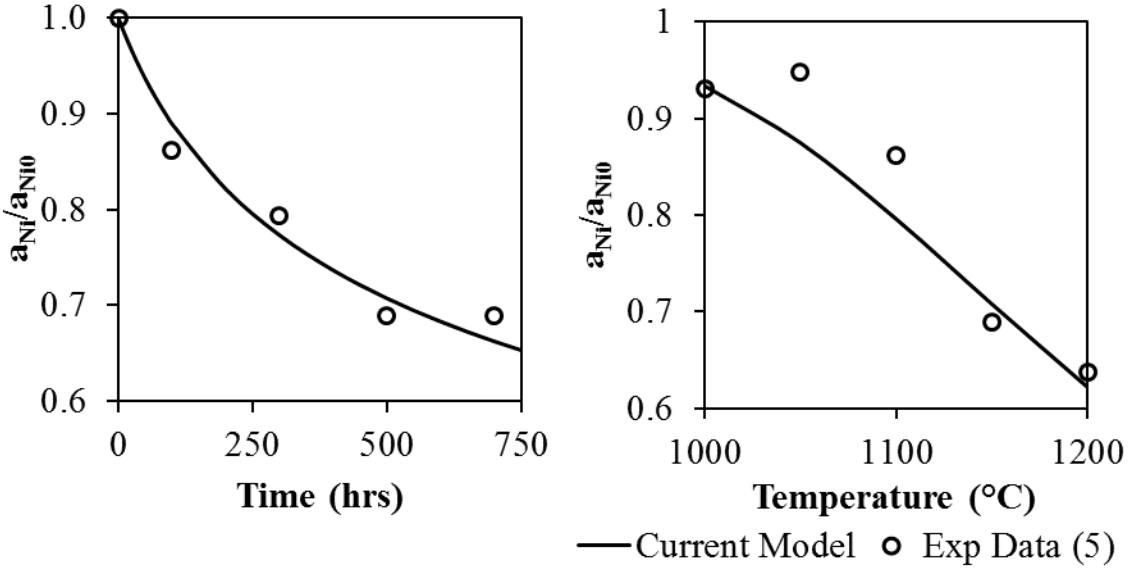

(a) (b)

Figure 2. Nickel surface area density change (a) as function of time at 1150°C (b) as a function of temperature at 500hrs (5).

A Bruggeman type model is used to estimate how the interfacial surface area density between electrode/electrolyte phases (a_s^{eff}) changes with the particle sizes of each phase:

$$a_s^{eff} = a_{s,0}^{eff}\left(\frac{d_{e,0}}{d_e} * \frac{V_e}{V_{Solid}} + \frac{d_{i,0}}{d_i} * \frac{V_i}{V_{Solid}}\right) \quad [13]$$

A similar model is applied to the pore diameter:

$$d_p = d_{p,0}\left(\frac{d_e}{d_{e,0}} * \frac{V_e}{V_{Solid}} + \frac{d_i}{d_{i,0}} * \frac{V_i}{V_{Solid}}\right) \quad [14]$$

Compared to pore size data from both Simwonis et al (6) and Kennouche et al (5), the model predicts the pore size growth relatively well as a function of time and temperature respectively (Figure 3). This is significant as it demonstrates that the model can predict microstructural property changes for two different initial microstructures (different phase volume fractions and initial grain sizes).

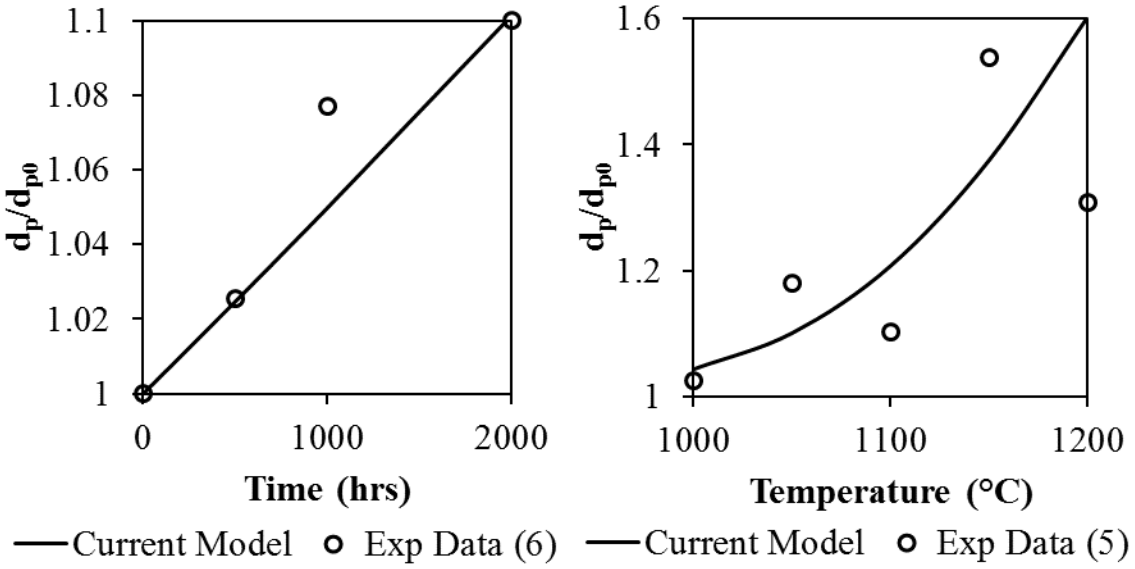

(a) (b)

Figure 3. Pore size change (a) as a function of time at 1000°C (6) (b) as a function of temperature at 500hrs (5).

Nickel conductivity data from Simwonis et al (6) is converted to an effective tortuosity via equation [3]. A power law equation is used for phase tortuosity evolution as a function of the average diameter of the phase (particle size or pore size):

$$\tau_\phi = \tau_{\phi,0}\left(\frac{d_\phi}{d_{\phi,0}}\right)^{n_\tau} \quad [15]$$

For an exponent of $n_\tau = 1.5$, the coarsening model prediction of the conductivity of Nickel as a function of time compares quite well with the experimental data (Figure 4).

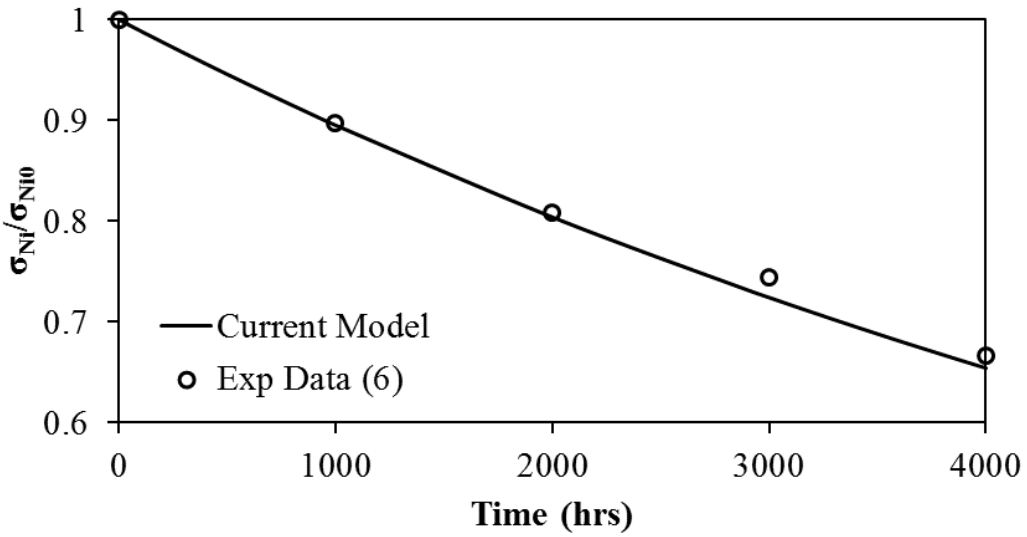

Figure 4. Nickel conductivity as a function of time at 1000°C (6).

Application

The multi-physics model is applied to the button cell depicted in Figure 1. A fitting procedure is carried out to approximate kinetic properties at 700, 750 and 800°C only. Data at three temperatures were used in order to establish that the parameters had an Arrhenius dependence on temperature. This procedure is part of a separate study that is exploring the minimum requirements from experiments to fully calibrate a model (7) (8). For future studies, data from only two different temperatures may be necessary. After repeating this process for each temperature, Arrhenius equations are derived from the fitted parameters. The parameters obtained with a minimum R^2 value of 0.9994 are shown in Table 2. These equations are then applied back into the model and performance predictions for additional temperature of 650 and 850°C are produced and compared to the baseline experimental data.

Table 2. Arrhenius equation parameters for kinetic properties ($\phi = A\exp(E_v/\kappa T)$)

Parameter	$E_V\ (eV)$	A	**Value at 800°C**	**Value at 850°C**
$C_{DL,a}$	0.439	$4.349\ F/m^2$	$376.1\ F/m^2$	$464.6\ F/m^2$
$C_{DL,c}$	-1.708	$0.144\ F/m^2$	$0.911\ F/m^2$	$0.839\ F/m^2$
$i_{0a}l_{TPB,a}$	0.590	$1.603E12\ A/m^2$	$2.71E9\ A/m^2$	$3.60E9\ A/m^2$
$i_{0c}l_{TPB,c}$	2.329	$1.749E20\ A/m^2$	$2.02E9\ A/m^2$	$6.19E9\ A/m^2$
σ_{YSZ}	0.115	$0.8675\ 1/\Omega m$	$0.250\ 1/\Omega m$	$0.264\ 1/\Omega m$

Predictions of impedance compared to the experiments at each temperature are shown in Figure 5 with similar comparisons for polarization curves shown in Figure 6. The model produces good predictions of the experimental performance data, even for temperatures which were not directly calibrated. It should also be noted that little attention was paid to the fit with polarization and power data during calibration. Simply

fitting the impedance data was enough to produce relatively accurate polarization predictions as well. This is probably because the baseline parameters taken from Yang et al (7) were for a similar button cell. This also suggests that the average microstructural properties obtained from the reconstruction of PFIB data are reasonable estimates of the bulk properties, specifically pore tortuosity which influences the limiting currents and peak power.

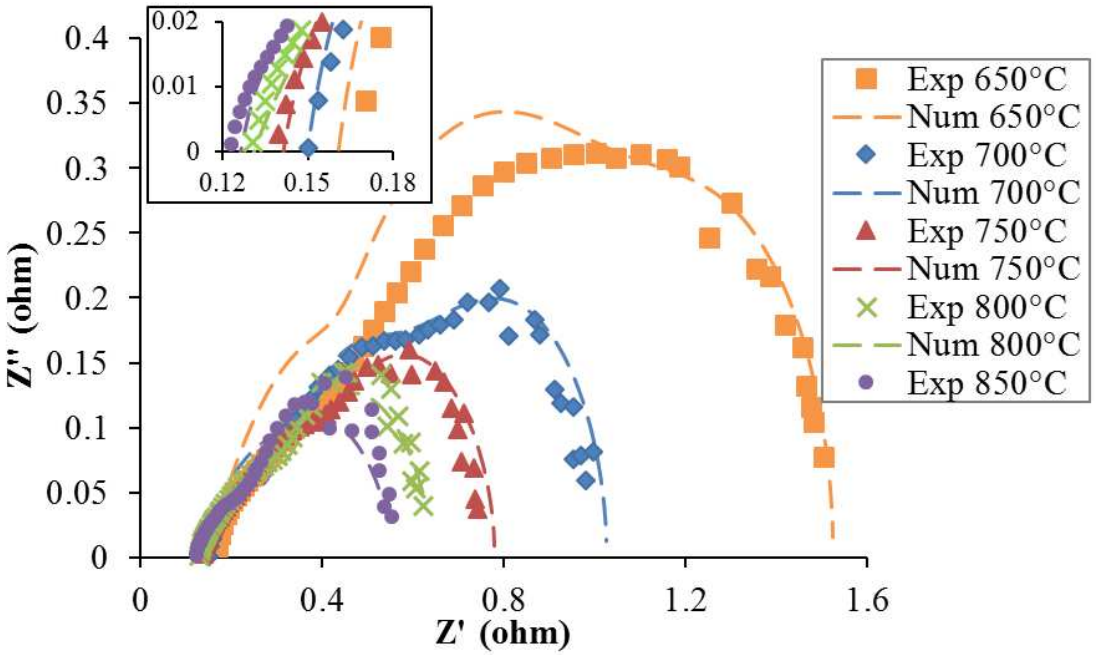

(b)

Figure 5. Baseline impedance measurements from 650-850°C compared to corresponding model performance predictions (a) Bode plots and (b) Nyquist plots.

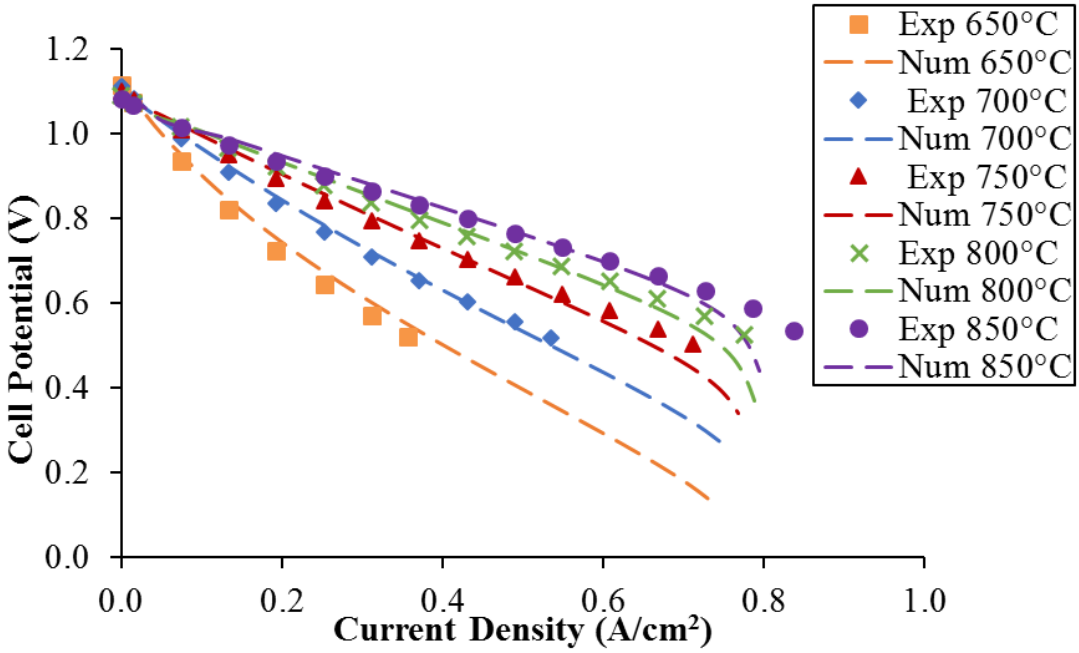

Figure 6. Baseline polarization curves from 650-850°C compared to corresponding model performance predictions.

Results and Discussion

With temperature dependence now in place for coarsening and for electrochemical kinetics, simulations of the button cell are carried out with performance data being generated every 5,000hrs of operation time out to 40,000hrs with smaller intervals also taken during the first 5,000hrs (0, 100, 250, etc.). This is repeated for operating temperatures of 750, 800 and 850°C. Examples of the polarization and power density curves produced over the course of 40,000 hours at 800°C are shown in Figure 7. As shown, the limiting current and peak power decrease significantly with operation time, while the degradation is subtle at lower current densities (less than 0.4 A/cm^2).

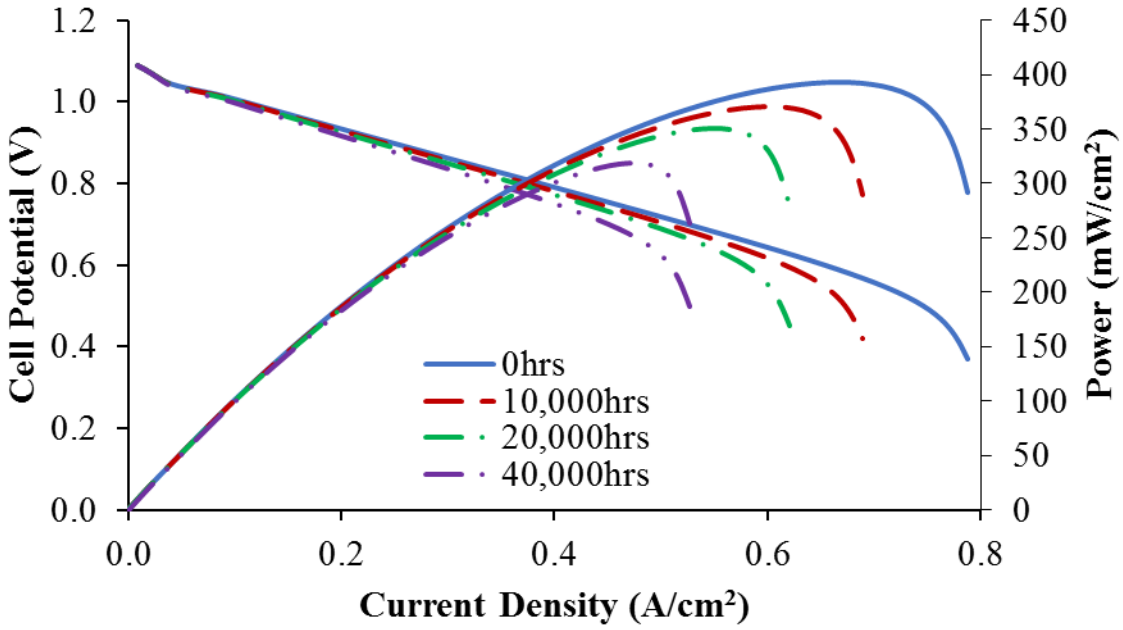

Figure 7. VI and power curves produced by model for an operating temperature of 800°C over the course of 40,000hrs.

From the VI-data, the cell voltage at 0.25 A/cm^2 as a function of time is extracted for an operating temperature of 750°C and compared to experimental data in Figure 8. The cell tested here was not the same used to produce the baseline data, but did come from the same batch. Therefore, it is reasonable to assume that the microstructural properties and performance should be similar. As shown, the predicted rate of degradation due to coarsening is insignificant compared to the actual observed degradation rate (0.03 compared to 2.35%/1000hrs). The model predicts that with these operating conditions and initial microstructure, coarsening will cause an insignificant amount of degradation compared to other modes such as secondary phase formation or crack formation and propagation are not considered in the present model.

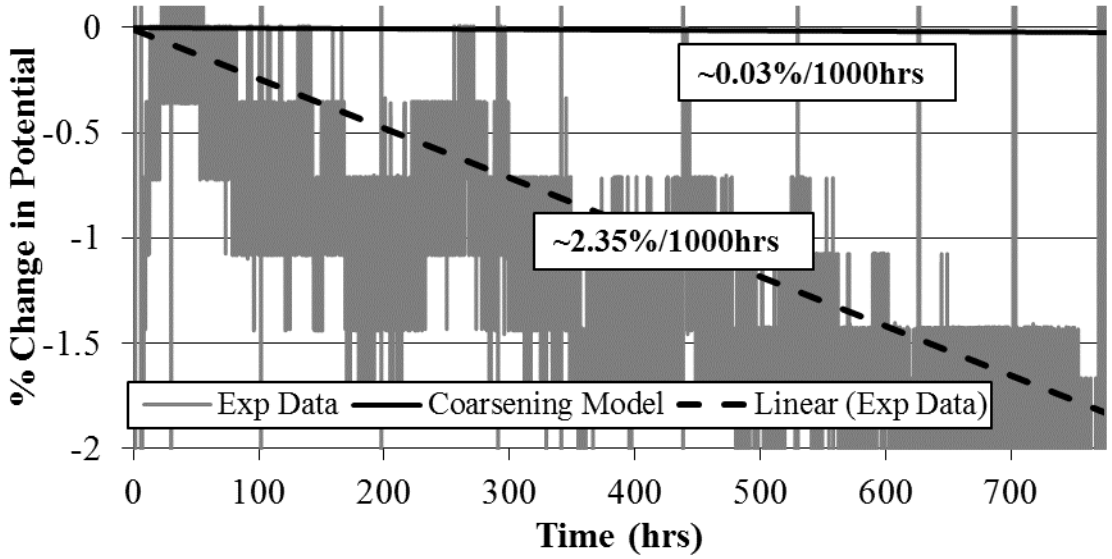

Figure 8. Button cell voltage at 750°C, 0.25 A/cm^2 as a function of time compared to coarsening model at the same conditions.

The cell potentials at 0.25 A/cm^2 as a function of time for each temperature simulated are presented in Figure 9. As shown, the operating temperature has a significant effect on the degradation rate due to coarsening. For each 50°C increase, the rate at which voltage decreases approximately doubles.

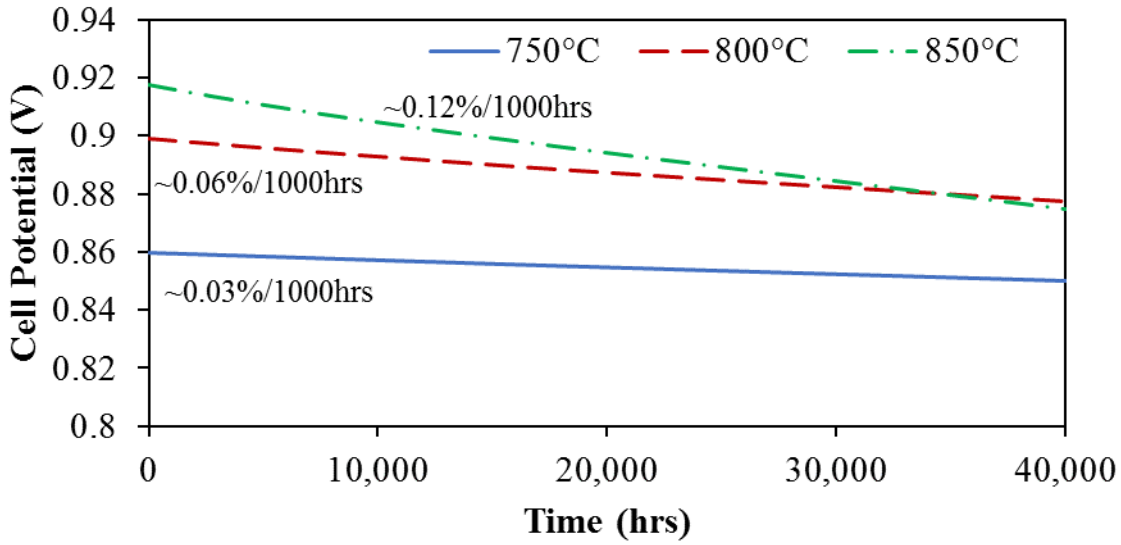

Figure 9. Model predictions of cell potential at 0.25 A/cm^2 at different operating temperatures as a function of time.

Conclusions

A particle coarsening model is implemented into a multi-physics model of a Ni/YSZ/LSM SOFC to predict degradation rates due to coarsening at different operating temperatures and initial microstructural compositions. The possible effects that an

applied current density may have on the coarsening rate are not considered. Property models are developed in conjunction with a particle coarsening model and microstructural properties taken from the literature. It is shown that these empirical models can reasonably predict how properties such as TPB density and phase conductivity evolve depending on average particle size and phase volume fractions. These models could be applied to any general microstructure. Microstructural and performance data from a commercial cell are applied to a multi-physics model to obtain temperature dependence relations for certain parameters such as exchange current density and double layer capacitance. This cell is then used as a baseline for subsequent investigations. Combining with the coarsening model, performance simulations of the baseline are performed for multiple temperatures and initial microstructure properties applying the coarsening model out to 40,000hrs of operation. Experimental measurements of cell potential for ~775hrs at 750°C and 0.25 A/cm^2 are compared to model predictions for similar operating conditions. For these conditions, evaluation of the results suggest that coarsening will account for very little of the degradation rate. The model does predict, however, that increasing operating temperature significantly increases the degradation. An increase of 50°C will results in a degradation rate due to coarsening which is approximately twice as large. This finding may have significant consequences for large planar cells/stacks where there are usually large temperature variations.

Acknowledgments

This product was prepared as an account of work sponsored by an agency of the United States Government. Neither the United States Government nor any agency thereof, nor any of their employees, makes any warranty, express or implied, or assumes any legal liability or responsibility for the accuracy, completeness, or usefulness of any information, apparatus, product, or process disclosed, or represents that its use would not infringe privately owned rights. Reference therein to any specific commercial product, process, or service by trade name, trademark, manufacturer, or otherwise does not necessarily constitute or imply its endorsement, recommendation, or favoring by the United States Government or any agency thereof. The views and opinions of authors expressed therein do not necessarily state or reflect those of the United States Government or any agency thereof."

This project was supported in part by an appointment to the Internship/Research Participation Program at the National Energy Technology Laboratory, U.S. Department of Energy, administered by the Oak Ridge Institute for Science and Education through an interagency agreement between the U.S. Department of Energy and NETL.

References

1. S. P. Jiang, *J. Material Science*, **38**(18), 3775 (2003).
2. H. Tu and U. Stimming, *J. Power Sources*, **127**(1), 284 (2004).
3. J. H. Kuo, et al, *J. Solid State Chem.*, **87**(1), 55 (1990).
4. D. Kennouche, et al, *J. Electrochem. Soc.*, **160**(11), F1293 (2013).
5. D. Kennouche, et al, *J. Power Sources*, **307**, 604 (2016).

6. D. Simwonis, et al, *Solid State Ionics*, **132**, 241 (2000).
7. T. Yang, et al, "Prediction of SOFC Performance with or without Experiments: A Study on Minimum Requirements for Experimental Data", *Int. J. Electrochem. Sci.,* (2017).
8. T. Yang, et al, *ECS Transactions*, **68**(1), 2397 (2015)
9. H. Finklea, et al, *J. Electrochem. Soc*., **160**(9), F1055 (2013).
10. S. R. Pakalapati, et al, *Solid State Ionics*, **258**, 45 (2014).
11. W. G. Bessler, et al, *Electrochemica Acta*, **53**(4), 1782 (2007).
12. S. C. DeCaluwe, et al, *J. Electrochem. Soc*., **155**(6), B538 (2008).
13. S. Gewies and W. G. Bessler, *J. Electrochem. Soc*., **155**(9), B937 (2008).
14. M. Matyka, et al, *Physical Review E*, **78**(2), 026306 (2008).
15. M. Doyle, et al, *J. Electrochem. Soc.*, **143**(6), 1890 (1996).
16. F. N. Cayan, et al, *J. Power Sources*, **192**(2), 467 (2009).
17. H. Yakabe, et al, *J. Power Sources*, **86**(1), 423 (2000).
18. F. Elizalde-Blancas, *Modeling issues for solid oxide fuel cells operating with coal syngas*, PhD Thesis, West Virginia University, Morgantown, WV (2009).
19. S. R. Pakalapati, *A new reduced order model for solid oxide fuel cells*, PhD Thesis, West Virginia University, Morgantown, WV (2006).
20. M. Palcut, *Solid State Ionics*, **202**(1), 6 (2011).
21. P. Shewmon and M. Janßen, *Diffusion in Solids*, Springer, 2016.
22. F. Abdeljawad, et al, *J. Power Sources*, **250**, 319 (2014).
23. L. Holzer, et al, *J. Power Sources*, **196**(3), 1279 (2011).
24. Y. Liu, *Solid State Ionics*, **206**, 97 (2012).
25. S. P. Jiang and W. Wang, *Solid State Ionics*, **176**(13), 1185 (2005).

Nomenclature

Variable	Description	Unit
a_s	Surface area density	m^2/m^3
C_{DL}	Double layer capacitance	F/m^2
c_ϕ	Molar density of species ϕ	mol/m^3
D_ϕ	Diffusion coefficient for species ϕ	m^2/s
d_ϕ	Particle diameter for species ϕ	m
E_A	Activation energy	eV
F	Faraday's constant	C/mol
i_F	Faradaic current density	A/m^3
i_0	Exchange current density	A/m^3
K_D	Surface diffusion coefficient	m^4/s
l_{TPB}	Triple phase boundary density	m/m^3
M_ϕ	Molecular weight of species ϕ	g/mol
n	Number of electrons exchanged (2 in this study)	
P_ϕ	Partial pressure of species ϕ	
R	Ideal gas constant	
S_ϕ	Source term for species ϕ	mol/m^3s
T	Temperature	K
t	Time	s
V	Volume fraction	
y_ϕ	Mass fraction of species ϕ	

α	Symmetry factor (0.5 for this study)	
β_ϕ	$1-\left(\frac{M_\phi}{\sum_i y_i M_i}\right)^{0.5}$	
η	Overpotential	V
κ	Boltzmann's constant	eV/K
σ	Conductivity	$1/\Omega m$
τ	Tortuosity	
φ	Local potential	V
	Sub/superscripts	
0	Initial or bulk value	
a	Pertaining to anode	
c	Pertaining to cathode	
e	Pertaining to electronic conducting material	
eff	Effective value	
eq	Equilibrium value	
i	Pertaining to ionic conducting material	
K	Knudsen	
m	Molecular	
p	Pertaining to pore or gas phase	
ϕ	Generic species or parameter	